Supplementary Information (SI) for Materials Horizons.
This journal is © The Royal Society of Chemistry 2025

Supplementary materials

Fully hardware-oriented physical reservoir computing using 3D vertical resistive switching memory with different bottom electrodes

Jihee Park[a], Gimun kim[a], and Sungjun Kim*[a]

[a] *Division of Electronics and Electrical Engineering, Dongguk University, Seoul 04620, South Korea.*
[b]

*Corresponding author: sungjun@dongguk.edu (S. Kim)

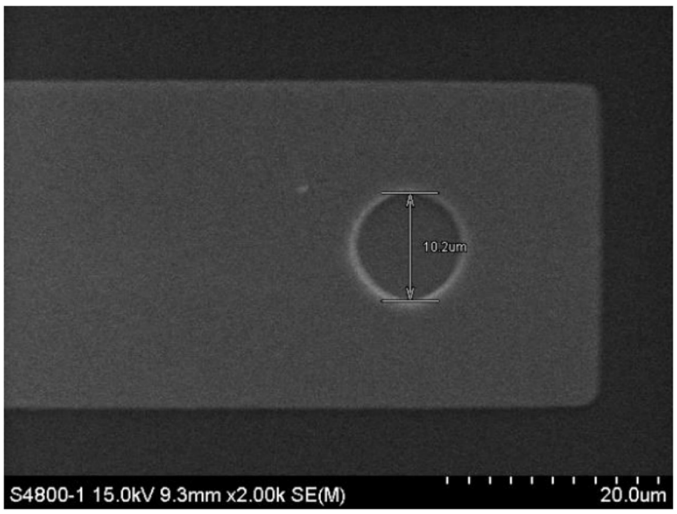

Fig. S1 Circle pattern of the hole in the resistive switching region.

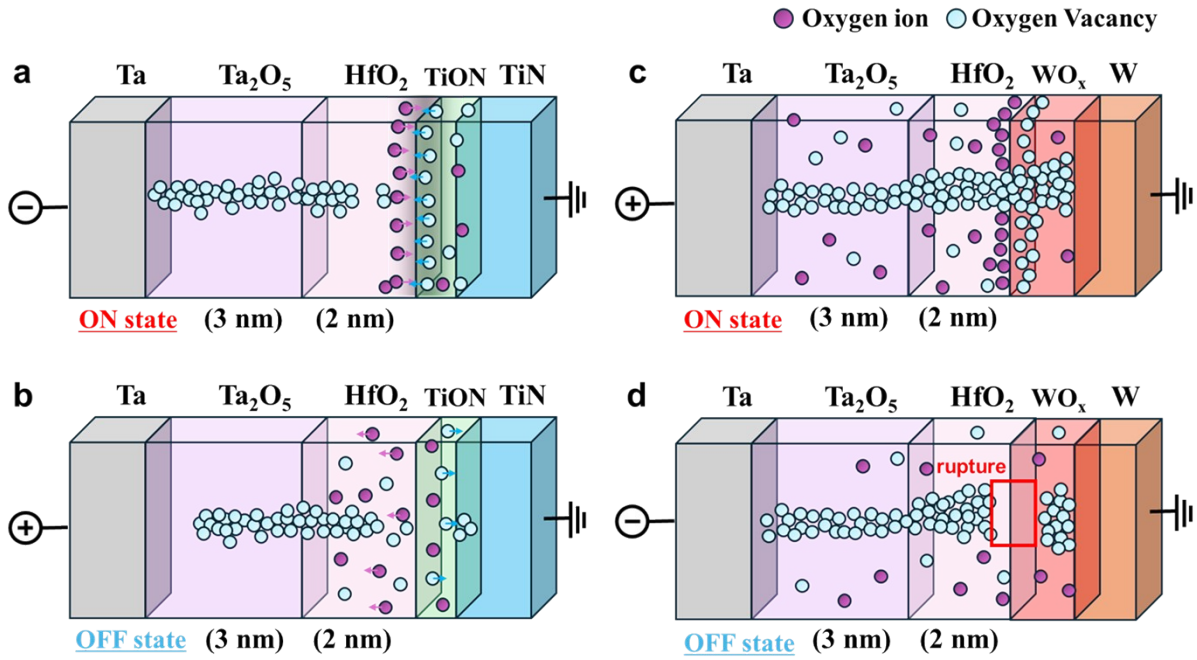

Fig. S2 Schematics diagram of filament formation and rupture process of Ta/Ta_2O_5/HfO_2/TiN device for a) LRS state, and b) HRS state, and Ta/Ta_2O_5/HfO_2/W device for c) LRS state, and d) HRS state.

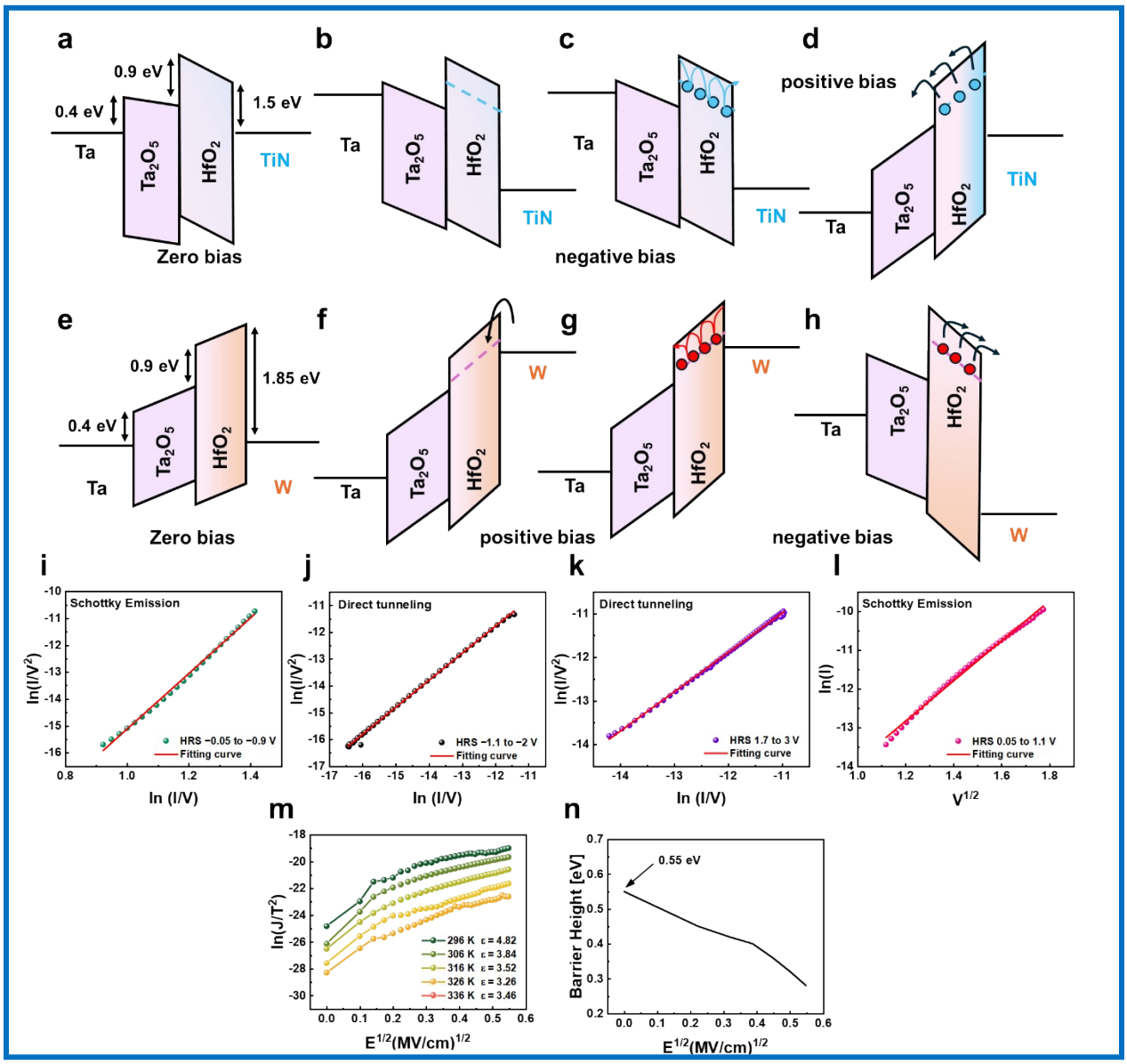

Fig. S3 Schematic diagram showing the switching mechanism: a) Schematic band diagram of the device with a TiN bottom electrode under zero bias condition. The bulk HfO_2 layer contains 1.0 eV deep traps, corresponding to the energy difference between the oxygen vacancy level and the conduction band edge. In localized regions, additional 0.6 eV shallow traps coexist with the deep traps. b) Under low negative bias, the injected electrons are transported through a trap-to-trap hopping mechanism. c) Once the 1.0 eV traps are fully occupied, the Poole–Frenkel (P–F) conduction effect emerges under a high electric field, effectively lowering the trap depth and enhancing conduction. d) When a low positive bias is applied, electrons trapped in the HfO_2 layer are detrapped. Simultaneously, carrier injection from the TiN electrode is suppressed by the Schottky barrier, returning the device to the HRS. e) Schematic band diagram of the device with a W bottom electrode under zero bias condition. f) Under low positive bias, the injected electrons are transported through the hopping conduction mechanism between trap states. g) Under high electric field, the P–F effect emerges as the trap depth becomes effectively shallower, enhancing carrier transport. h) Under low negative bias, electrons in the trap states are detrapped, and carrier injection from the W electrode is suppressed by the Schottky barrier, switching the device back to the HRS. i) Schottky emission fitting that models the relationship between ln(I) and sqrt(V) in the range from −0.05 to −0.9 V. j) Direct tunneling fitting that models the relationship between $\ln(I/V^2)$ and ln(I/V) in the range from −1.1 to −2 V. k) Direct tunneling fitting that models the relationship between $\ln(I/V^2)$ and ln(I/V) in the range from 1.7 to 3 V. l) Schottky emission fitting that models the relationship between ln(I) and sqrt(V) in the range from 0.05 to 1.1 V. m) Experimental data were plotted according to the Schottky equation (Eq.1) in the low field region (E< ~0.3 MV/cm) from 296 K to 336 K. n) the change Φ_B as a function of $E^{1/2}$.

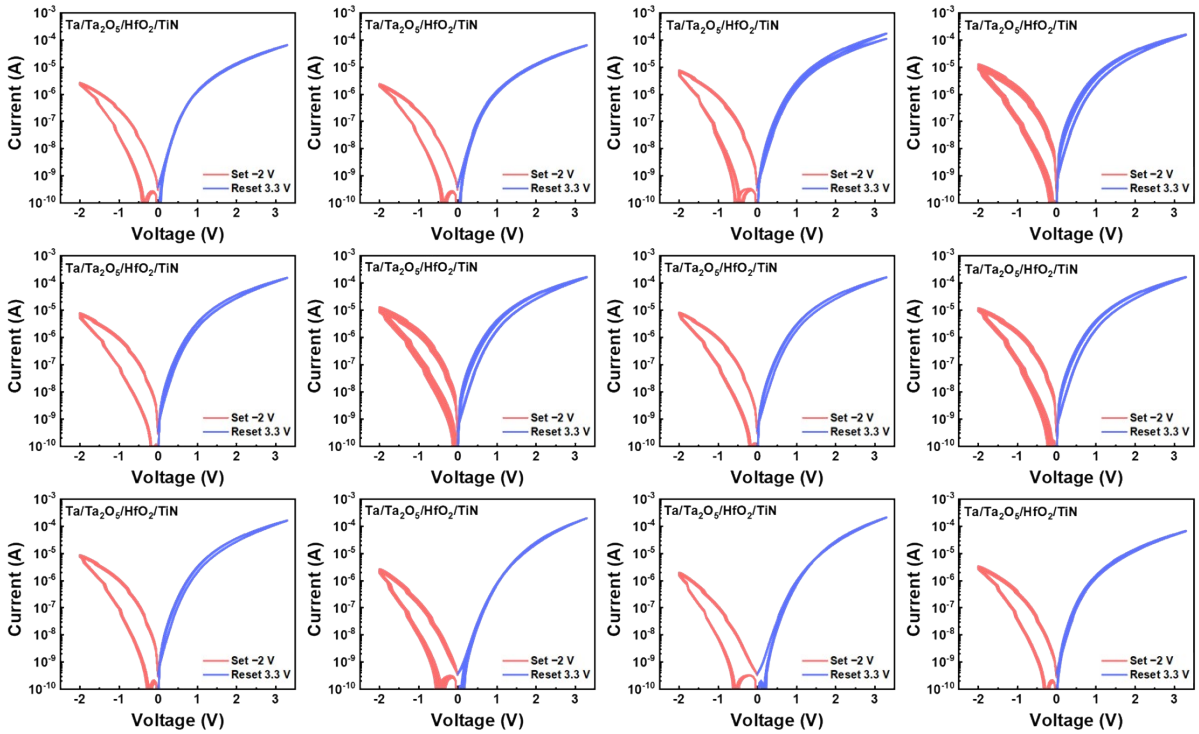

Fig. S4 device to device I-V characteristics of $Ta/Ta_2O_5/HfO_2/TiN$ cells.

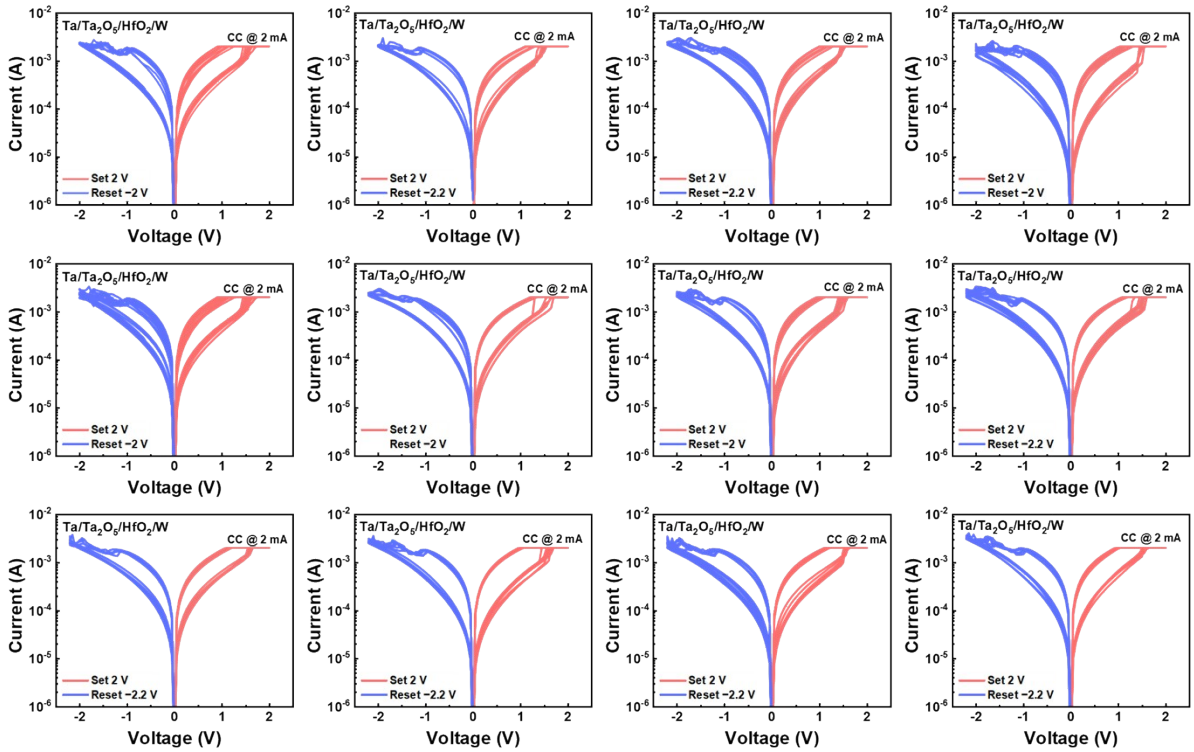

Fig. S5 device to device I-V characteristics of $Ta/Ta_2O_5/HfO_2/W$ cells.

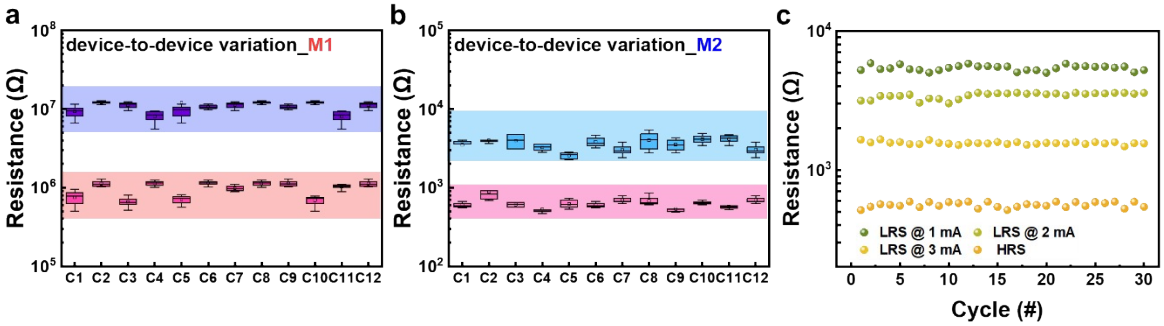

Fig. S6 a) Cell-to-cell variation of 12 randomly selected M1 device, and b) M2 device, and c) cycle-to-cycle variation of LRS and HRS over 30 switching cycles under compliance currents of 1 mA, 2 mA, and 3 mA.

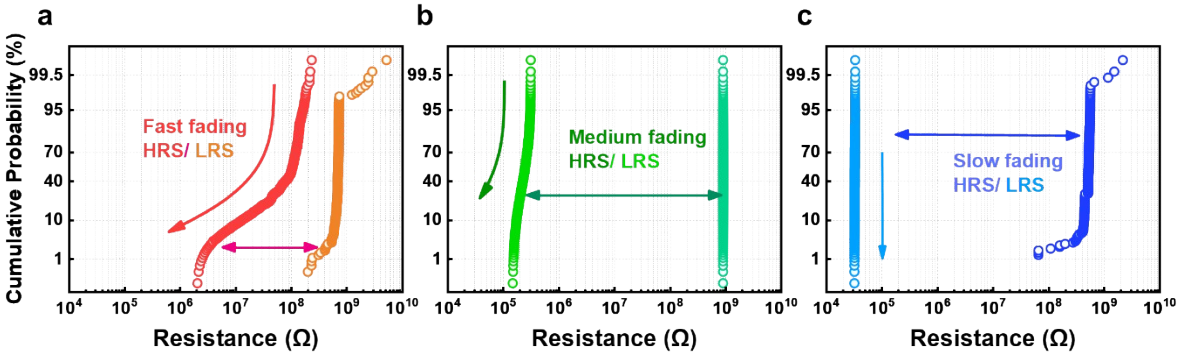

Fig. S7 a) Cumulative probability of the M1 device under a −2 V applied voltage, b) −3 V, and c) −4 V.

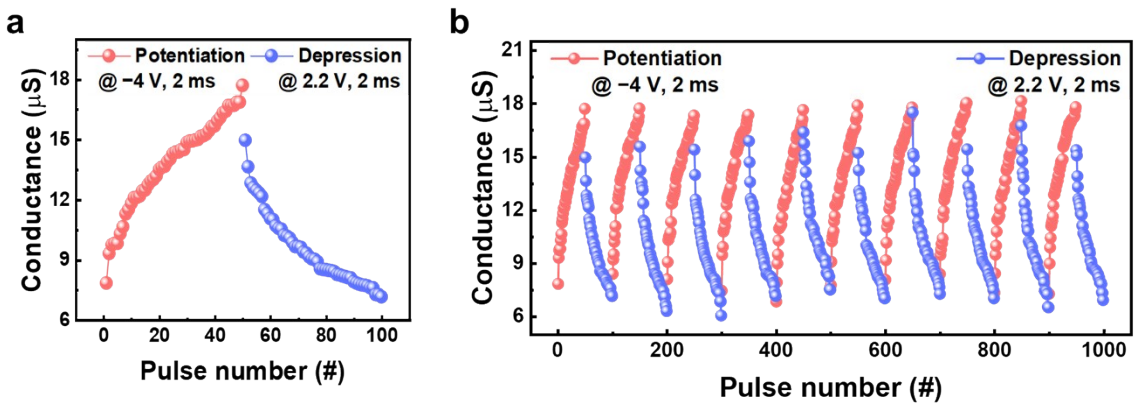

Fig. S8 a) Potentiation and depression (P&D) properties of an M1 memristor, and b) result after 10 cycles.

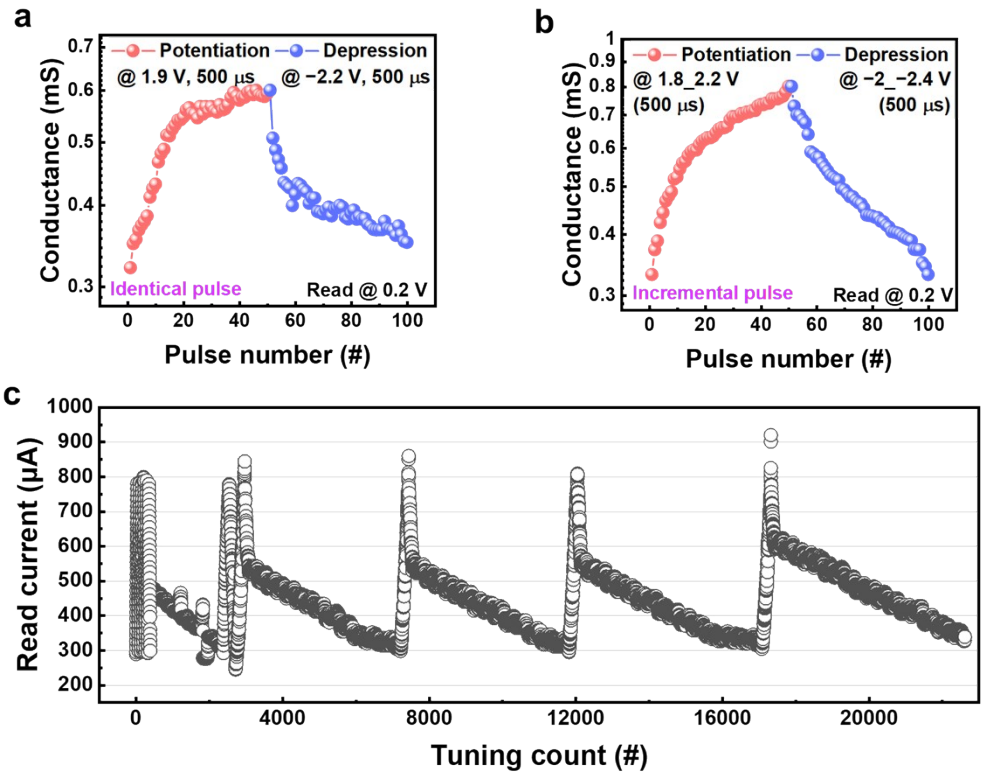

Fig. S9 P&D properties of an M2 memristor a) identical, b) incremental pulse, and c) the tunning process of ISPVA.

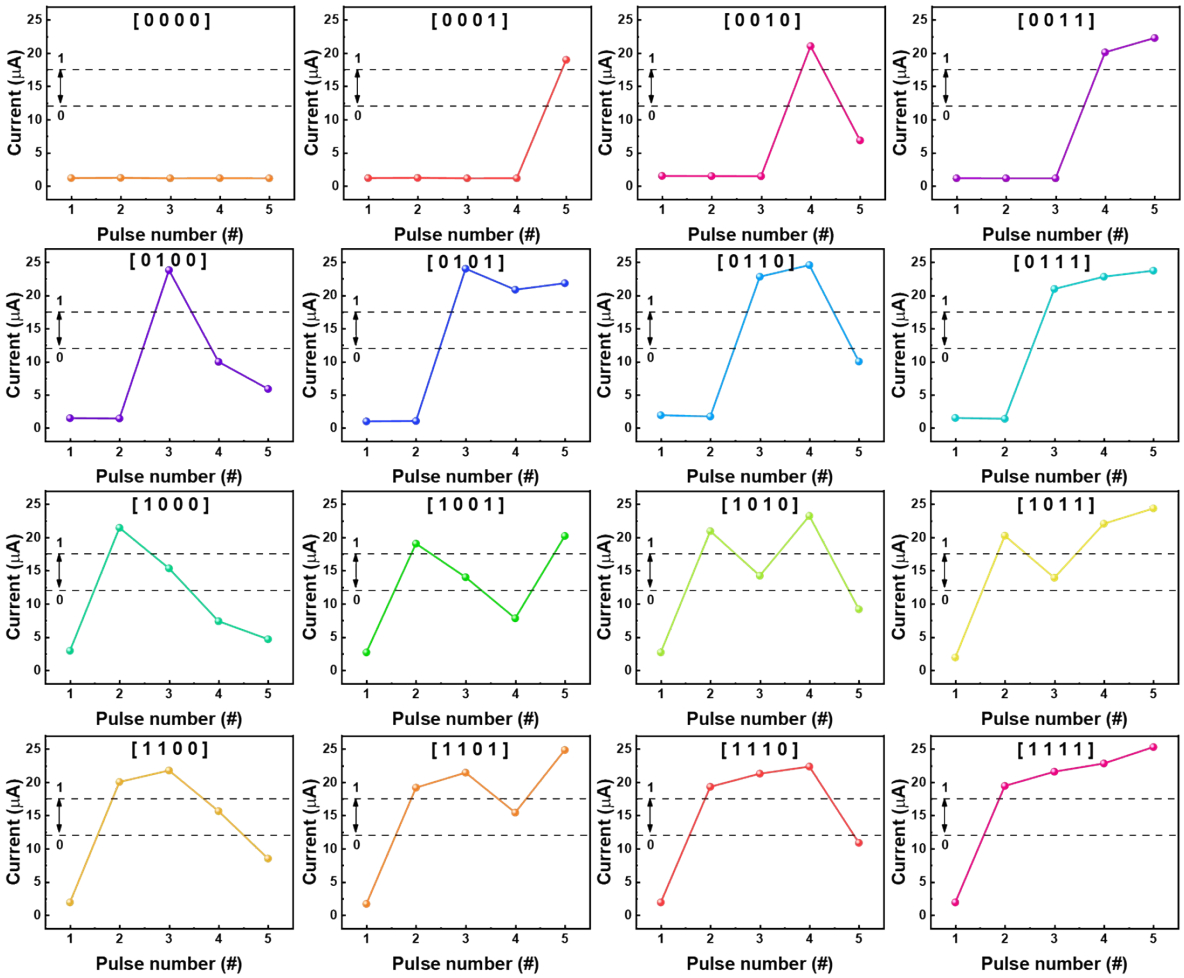

Fig. S10 Current responses of 16 states for 4-bit reservoir computing corresponding to input pulse streams ranging from [0000] to [1111] under low voltage application.

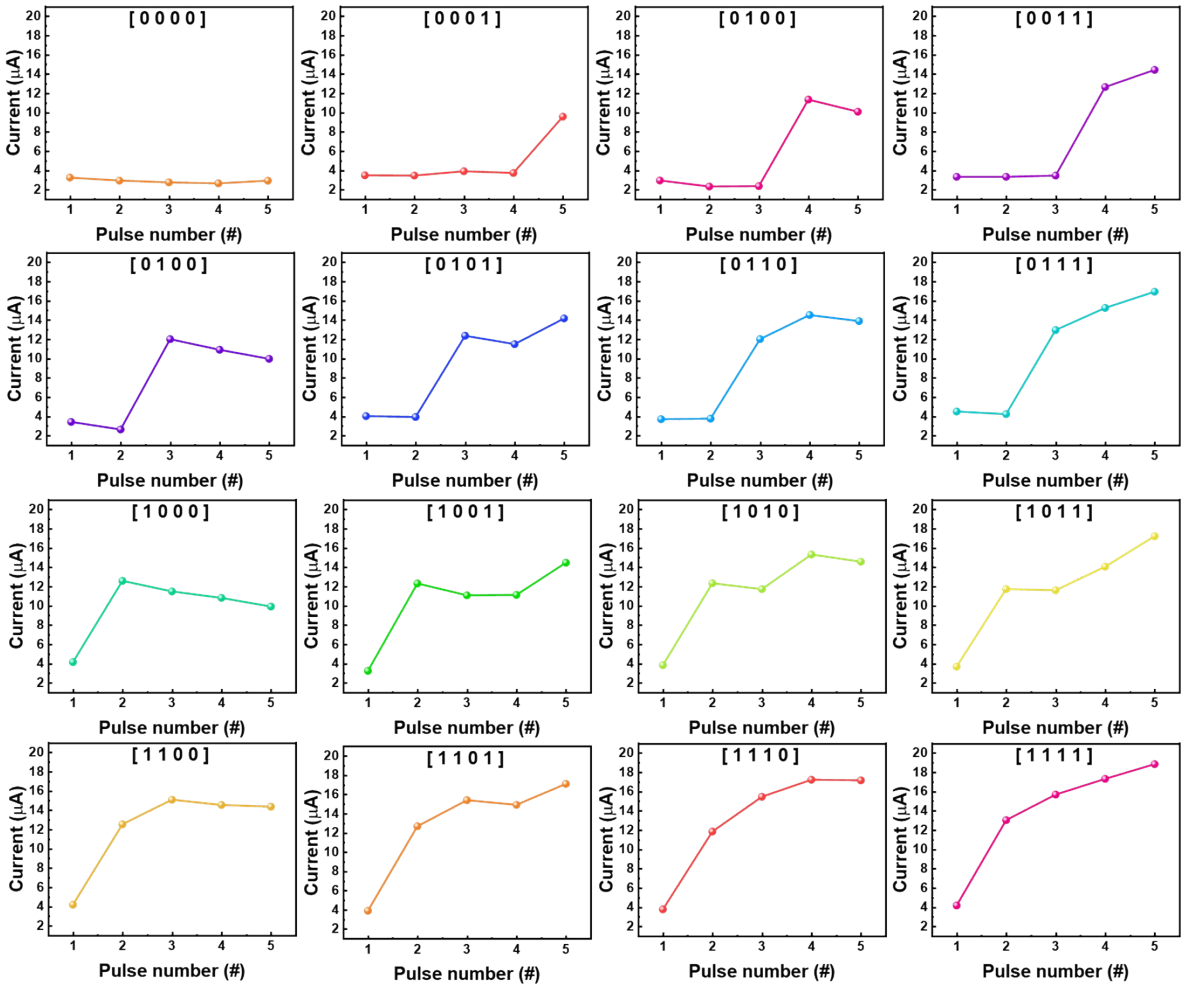

Fig. S11 Current responses of 16 states for 4-bit reservoir computing corresponding to input pulse streams ranging from [0000] to [1111] under high voltage application.

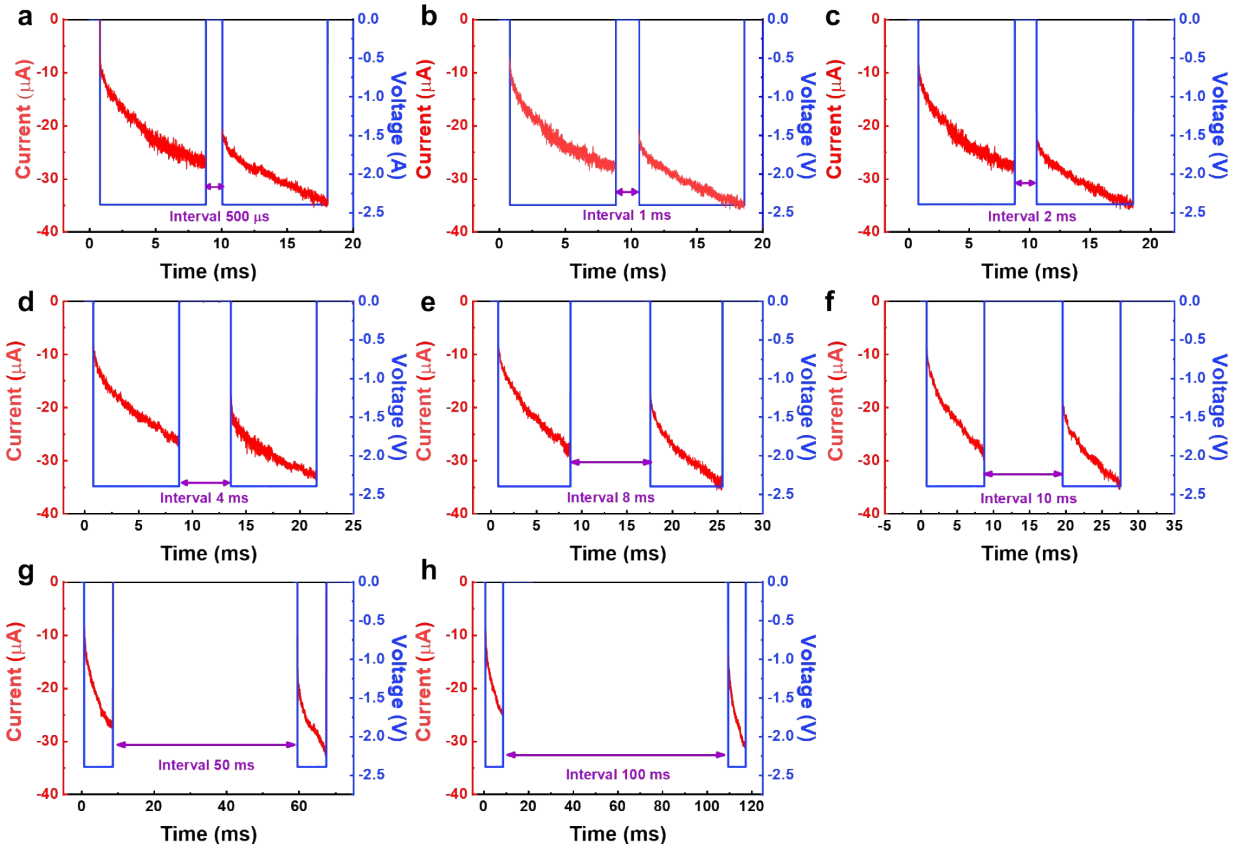

Fig. S12 PPF characteristics with a pulse interval of a) 500 μs, b) 1 ms, c) 2 ms, d) 4 ms, e) 8 ms, f) 10 ms, g) 50 ms, and h) 10 ms, at a fixed amplitude of −2.4 V.

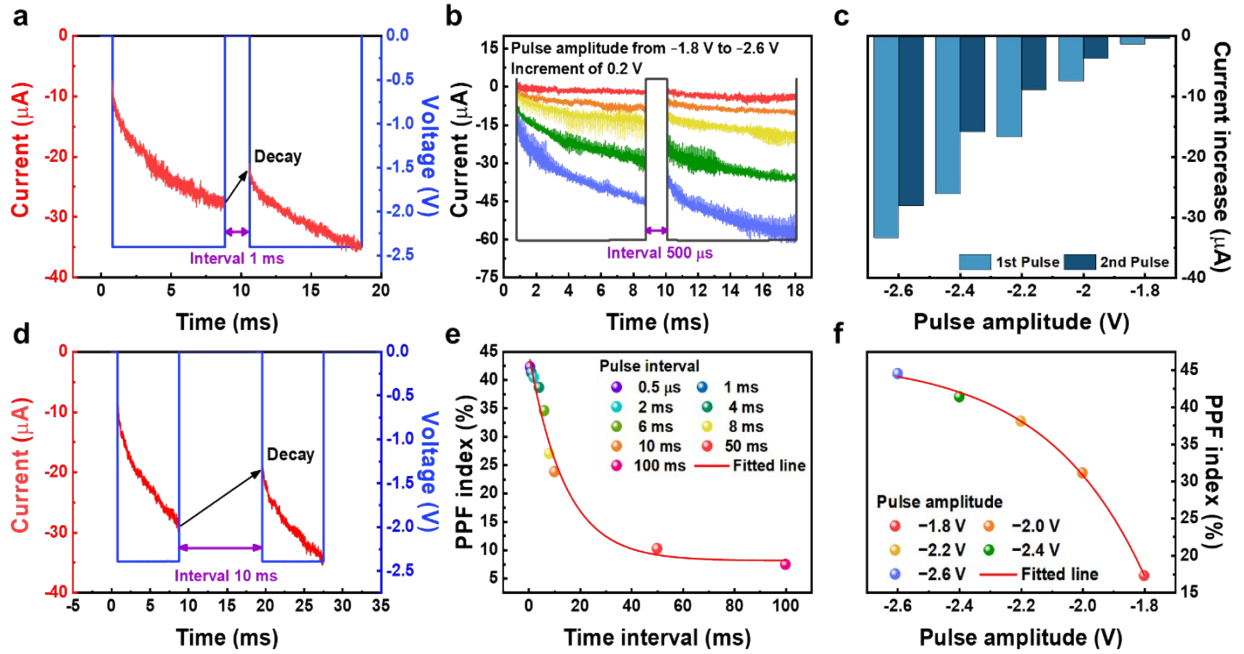

Fig. S13 a) PPF characteristics with a pulse interval of a 1 ms, d) 10 ms, at a fixed amplitude of −2.4 V. b) PPF characteristics with pulse amplitudes ranging from −1.8 V to −2.6 V, at a fixed interval time of 1 ms. c) Current increase at pre-pulse and post-pulse across varying amplitudes. e) PPF index as a function of interval time, ranging from 0.5 μs to 100 ms. f) PPF index as a function of pulse amplitude, ranging from −1.8 V to −2.6 V.

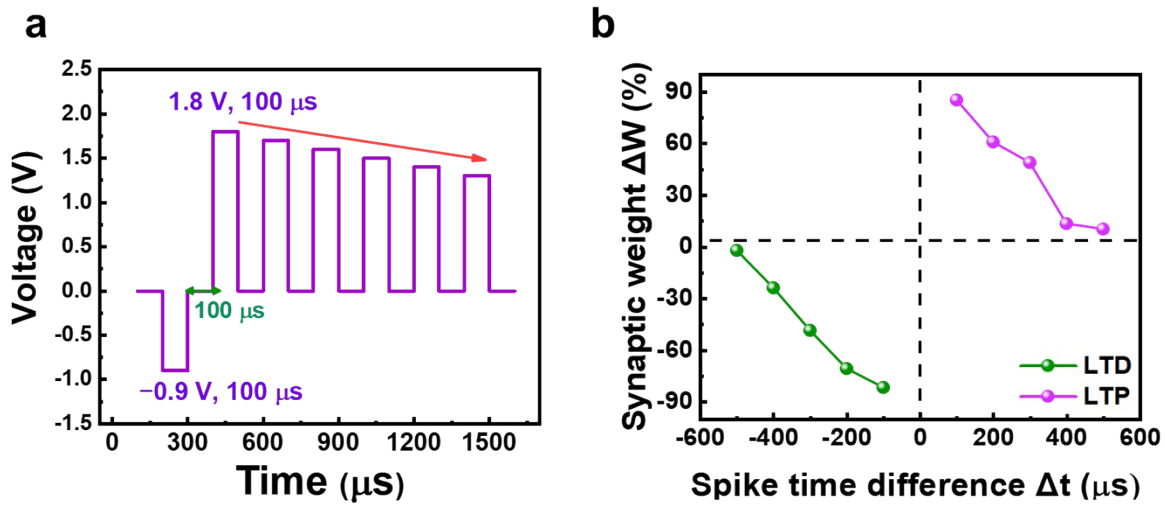

Fig. S14 a) Pulse scheme for STDP measurement at Δt = 100 μs, and b) STDP measurement results showing synaptic potentiation and depression induced by positive and negative pulses.

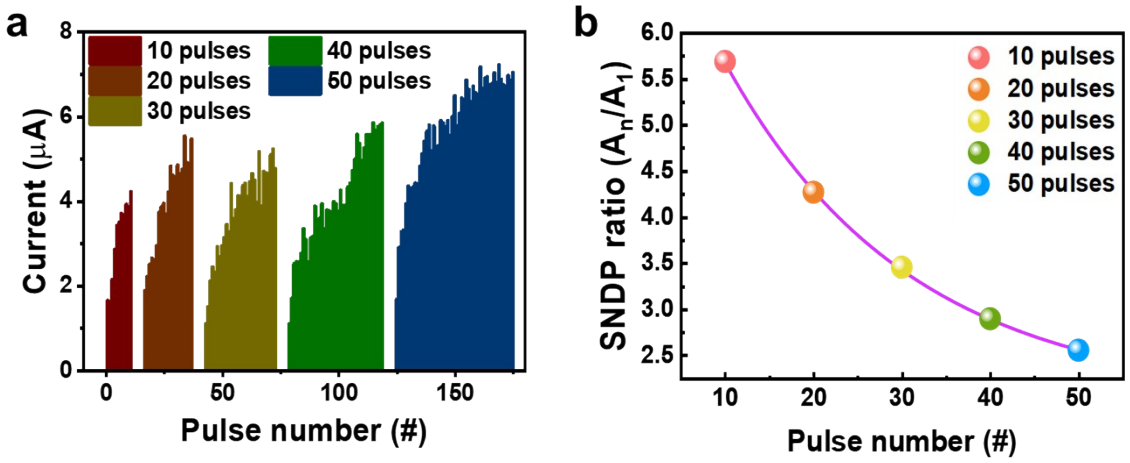

Fig. S15 a) Conductance response of the Ta/Ta_2O_5/HfO_2/TiN device at different pulse number during the application of ten set pulses. b) EPSC gain plotted by various number of pulses in set pulses.

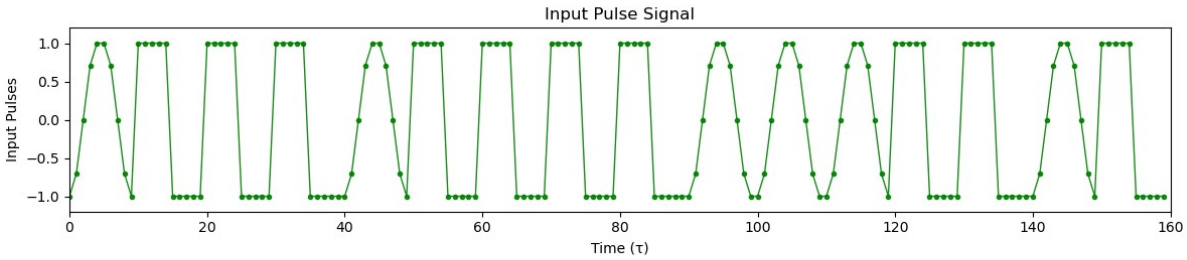

Fig. S16 Input generation for classification sine and squarewaveforms.